Phase Behavior in Thin Films of Cylinder-Forming Block Copolymers

A. Knoll,[1] A. Horvat,[1] K. S. Lyakhova,[2] G. Krausch,[1] G. J. A. Sevink,[2] A. V. Zvelindovsky,[2] and R. Magerle[1,*]

[1]*Physikalische Chemie II, Universität Bayreuth, D-95440 Bayreuth, Germany*

[2]*Leiden Institute of Chemistry, Leiden University, P.O. Box 9502, 2300 RA Leiden, The Netherlands*

(Received 4 September 2001; published 27 June 2002)

We have experimentally determined a phase diagram for cylinder-forming polystyrene-*block*-polybutadien-*block*-polystyrene triblock copolymer in thin films. The phase behavior can be modeled in great detail by dynamic density functional theory. Deviations from the bulk structure, such as wetting layer, perforated lamella, and lamella, are identified as surface reconstructions. Their stability regions are determined by an interplay between surface fields and confinement effects.

DOI: 10.1103/PhysRevLett.89.035501 PACS numbers: 61.25.Hq, 61.20.Ja, 68.37.Ps, 68.55.Jk

Ordered fluids are a fascinating class of materials as they combine crystal-like order on mesoscopic length scales with liquidlike disorder on microscopic scales. As a typical example, amphiphilic block copolymers tend to self-assemble into ordered microstructures with characteristic lengths determined by the molecular size, i.e., in the 10–100 nm range [1]. The microdomain structure in the bulk is determined mainly by the molecular architecture, in particular the ratio of block lengths and the interaction between the two components (blocks). At interfaces and in thin films an additional driving force for structure formation exists, because one component typically has a lower interfacial energy than the other. This phenomenon belongs to a class of *interfaces of modulated phases* [2,3]. Related phenomena of two-component systems are wetting and surface enrichment, surface directed spinodal decomposition [4], and surface-induced ordering and orientation [5,6]. Recently, we have shown that in analogy to surface reconstructions of crystal surfaces the near-surface structure can deviate from the bulk structure in block copolymers as well [7]. In thin films, additional constraints exist. Here, the microdomain structure has to adjust to two boundary surfaces and a certain film thickness, which can be a noninteger multiple of the "natural" bulk repetition length. Both constraints together cause a complex and interesting phase behavior.

Based on the pioneering work by Anastasiadis *et al.* [6], numerous studies have dealt with thin films of lamellar block copolymers and two major effects have been identified [8]. The preferential attraction of one type of block to the surface (the surface field) causes the lamella to align parallel to the interfaces and the film form islands or holes (terraces) where the film thickness is a (half) integer multiple of the bulk lamella size.

While any cross section parallel to a lamella exhibits the same symmetry as a planar surface, the situation is more complex in the case of cylinder-forming systems. Here, a planar surface, regardless of its orientation, always breaks the symmetry of the bulk structure and the microdomain structure has to adjust. Indeed, a variety of deviations from the bulk structure have been observed near surfaces and in thin films such as a wetting layer [9], spherical microdomains [10], a perforated lamella [10], cylinders with necks [11], and more complicated structures [12,13]. Although various models have been developed to describe this behavior [14–17] (for summary, see Ref. [17]), modeling and experimental results agree qualitatively only in parts. It remains unclear which of the reported phenomena are specific to the particular system and/or route of film preparation and which are general behavior. As a result, no general agreement is reached about the underlying fundamentals.

In this Letter we present a unifying description of these phenomena. With experiments and computer simulations based on dynamic density functional theory (DDFT) we show that the phase behavior in thin films of cylinder-forming block copolymers is dominated by surface reconstructions. Their stability regions are determined by the surface field and the film thickness and we show how these two constraints interact.

As a model system we have chosen thin films of a cylinder-forming polystyrene-*block*-polybutadiene-*block*-polystyrene (SBS) triblock copolymer swollen in chloroform vapor. SBS was obtained from Polymer Source Inc. with molecular weights of blocks $M_{w,\mathrm{PS}} = 14\mathrm{k}$, $M_{w,\mathrm{PB}} = 73\mathrm{k}$, and $M_{w,\mathrm{PS}} = 15\mathrm{k}$ (PS is polystyrene, PB is polybutadiene). Thin SBS films were spun cast from toluene solution onto polished silicon substrates. In order to equilibrate (anneal) the microdomain structure, the films were exposed for 7 h to a controlled partial pressure p of chloroform vapor [18]. The total pressure was 1.3 ± 0.1 atm and the temperature was kept at $25.0 \pm 0.1\,^{\circ}\mathrm{C}$. The resulting microdomain structures were quenched via fast solvent removal. During annealing, the nonselective solvent, $CHCl_3$, acts as a plasticizer, which merely induces chain mobility. Within the studied range of $\tilde{p} = p/p_S$ (p_S is the partial pressure of saturated $CHCl_3$ vapor at 25.0 °C) the lateral spacing between two neighboring PS cylinders, a_0, decreases with increasing $\tilde{p}$ from $a_0 \approx 41$ to 39 nm, similar to Ref. [19].

During vapor annealing the films form terraces with thicknesses smaller and larger than the original thickness. We have determined the step heights using TappingMode™ scanning force microscopy (TM-SFM).

TM-SFM phase images were recorded along with the height images to map (via the difference in modulus) the lateral distribution of PS and PB near the film surface [20].

Figures 1(a) and 1(b) show TM-SFM phase images of two annealed SBS films with different initial film thicknesses. Both films have formed regions of well-defined film thickness as indicated by the height profile shown in Fig. 1(c). At the same time well-defined microdomain patterns have formed, which change systematically as a function of the gradually changing film thickness (at steps between terraces). In particular, boundaries between different structures correspond to height contour lines. A major fraction of the surface displays bright stripes, which are indicative of PS cylinders oriented parallel to the surface ($C_{\parallel}$). In thinner regions of the film two additional patterns are found: One is characterized by hexagonally ordered dark spots, indicative of PB microdomains in an otherwise continuous PS layer, i.e., a perforated PS lamella (PL). The slopes between neighboring terraces display a hexagonal pattern of bright dots, indicative of PS cylinders oriented perpendicular to the surface ($C_{\perp}$). Finally, the thinnest parts of the films display no lateral structure at all, indicative of either a disordered (dis) phase or a lamellar wetting layer (W). In thicker films, the sloped regions between terraces display stripes as well. Previous work has shown that the parallel orientation of PS cylinders continues through the depth of the film to the substrate [18,22]. We note that these phases were all reported earlier and for various experimental conditions and cylinder-forming block copolymers. In the present experiments, however, *all* phases appear in a *single* system and under identical experimental conditions. This finding indicates that the film thickness is an important control parameter.

In order to explore the role of the strength of the surface field, the above experiment was repeated as a function of solvent vapor pressure $\tilde{p}$ during annealing. With increasing $\tilde{p}$, the total polymer concentration, Φ_P, in the film decreases, which effectively reduces the interaction parameter between the two polymeric components and between the polymers and the confining surfaces. The experimental results are summarized in a phase diagram (Fig. 2) displaying the stability regions of the various phases as functions of $\tilde{p}$ and film thickness (after drying). Note that films annealed at larger $\tilde{p}$ shrink more in the vertical z direction upon drying than films prepared at smaller $\tilde{p}$.

The PL phase is predominantly observed in the lower terrace when the neighboring terrace forms the $C_{\parallel,2}$ phase. With increasing $\tilde{p}$, the area fraction of the lower terrace forming a PL decreases. For $\tilde{p} = 0.64$, 0.68, and 0.70 the area fraction is 90%, 80%, and 50%, respectively. For $\tilde{p} > 0.71$, no PL is observed. In thicker films only for $h \approx 60$ nm and $\tilde{p} = 0.66$, a small fraction, 10%, of the terraces forms a PL.

The assignment of surface patterns to distinct phases is corroborated by DDFT simulations of the complete thin film structure. We have used the MESODYN code [23] to simulate a melt of $A_3B_{12}A_3$ "molecules." Briefly, the block copolymer is modeled as a Gaussian chain with different beads A and B. For the bead-bead interaction potential a Gaussian kernel is used characterized by ε_{AB}. The film interfaces were treated as mask (M) with a corresponding bead-mask interaction parameter $\varepsilon_M = \varepsilon_{AM} - \varepsilon_{BM}$. The spatiotemporal evolution of bead densities $\rho_i(\vec{r}, t)$ is obtained using the complete free energy functional $F[\{\rho_i\}]$ and the chemical potentials $\mu_i = \partial F[\{\rho_i\}]/\partial \rho_i$. The Langevin diffusion equation is solved numerically starting from homogeneous densities. Appropriate noise

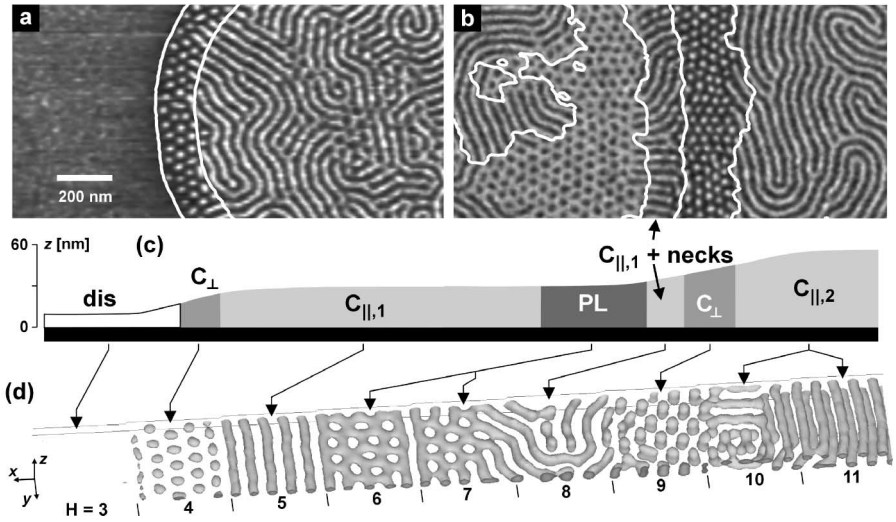

FIG. 1. (a,b) TM-SFM phase images of thin SBS films on Si substrates after annealing in chloroform vapor at $\tilde{p} = 0.62$. The surface is everywhere covered with an ≈10-nm-thick PB layer. Bright (dark) corresponds to PS (PB) microdomains below this top PB layer [21]. Contour lines calculated from the corresponding height images are superimposed. (c) Schematic height profile of the phase images shown in (a,b). (d) Simulation of an $A_3B_{12}A_3$ block copolymer film in *one* large simulation box of $[352 \times 32 \times H(x)]$ grid points with increasing film thickness $H(x)$, $\varepsilon_{AB} = 6.5$, and $\varepsilon_M = 6.0$. The latter corresponds to a preferential attraction of B beads to the surface. The isodensity surface $\rho_A = 0.5$ is shown.

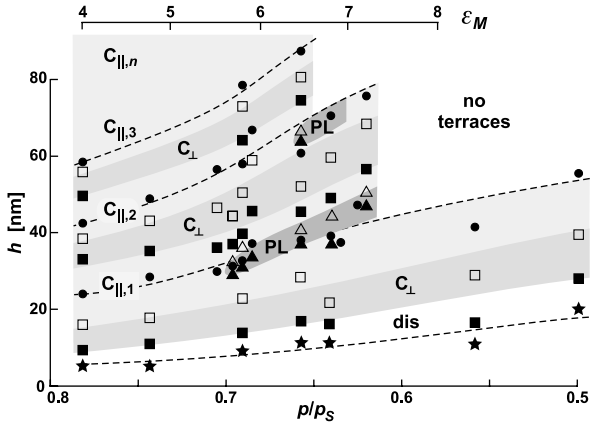

FIG. 2. Phase diagram of thin SBS block copolymer films on Si subtrates after annealing in chloroform vapor. Data are given for equilibrium film thicknesses of $C_{\parallel,n}$ (•) and "dis" (★) and for upper and lower bounds (open and closed symbols, respectively) of $C_\perp$ (□, ■) and PL (△, ▲) phases. The latter correspond to contour lines such as those shown in Figs. 1(a) and 1(b). All lines and areas are drawn to guide the eye.

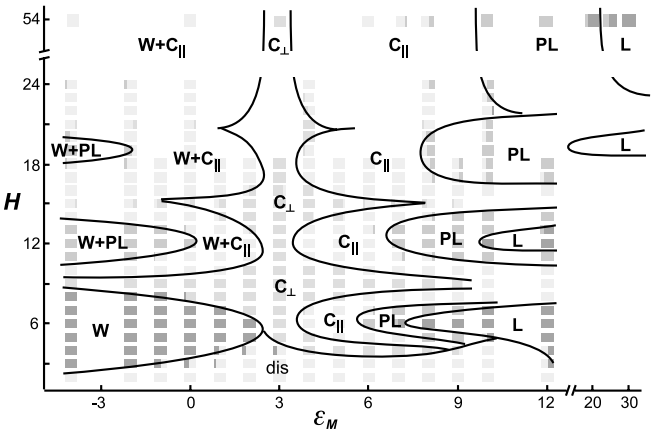

FIG. 3. Phase diagram of surface reconstructions of a $A_3B_{12}A_3$ block copolymer film calculated with MESODYN for $\varepsilon_{AB} = 6.5$. The boxes indicate where simulations have been done. The boxes with two shades of grey indicate that two phases coexist after the finite simulation time. Smooth phase boundaries have been drawn to guide the eye.

is added to the dynamics. We have done simulations with $\varepsilon_{AB} = 6.3$, 6.5, and 7.1 (in kJ/mol) and varied systematically the strength of the polymer/surface interaction ε_M and the film thickness H. We have used the parametrization of Ref. [15] and have followed the temporal evolution until significant changes no longer occurred. We chose to model the swollen SBS film as a melt to keep the total number of parameters as small as possible. The effect of the nonselective solvent $CHCl_3$ is modeled as an effective interaction parameter $\varepsilon_M = \varepsilon_M^{\text{melt}}\Phi_P$.

We find that modeling with $\varepsilon_{AB} = 6.5$ matches our experimental data best. Figure 1(d) shows the result of a simulation done in a wedge-shaped geometry. It exhibits exactly the same sequence of phases as the experimental data. Starting from a disordered phase (dis) for $H = 3$ grid units, spheres or very short upright cylinders, $C_\perp$, form ($H = 4$). These are followed by parallel cylinders, $C_{\parallel,1}$ ($H = 5$), a perforated lamella, PL ($H = 6$), a PL coexisting with $C_{\parallel,1}$ ($H = 7$), cylinders with ripples or necks ($H = 8$), then upright cylinders, $C_\perp$ ($H = 9$), and two layers of parallel cylinders, $C_{\parallel,2}$ ($H = 10$, 11, and 12). The film thickness at which phase transitions occur as well as the relative domain spacings are correctly predicted. The distance between next-nearest holes of the PL is found to be 1.15 times larger than the distance between next-nearest cylinders, $a_0 = 7.0 \pm 0.5$ grid units, of the $C_\parallel$ and the $C_\perp$ phase. We also observe this in our experiments [Fig. 1(b)].

For a systematic study of the influence of ε_M and H on the thin film structure we have done simulations in smaller boxes with $[32 \times 32 \times (H + 1)]$ grid points and a mask in the $z = 0$ plane. The structures found for $\varepsilon_{AB} = 6.5$ are summarized in a phase diagram shown in Fig. 3. The middle part of the phase diagram resembles the one reported for A_3B_6 diblock copolymers [15] but covers a much larger parameter space.

The simulation results match nicely the experimental phase diagram shown in Fig. 2. For a quantitative comparison of the two phase diagrams, one has to take into account that the film thickness relevant for structure formation is the thickness in the swollen state. Furthermore, we need to relate the vapor pressure, $\tilde{p}$, to the effective interaction parameter between the polymer blocks and the confining surface, ε_M. We assume that $\varepsilon_M = \varepsilon_M^{\text{melt}}\Phi_P$, where Φ_P can be estimated from the amount of shrinkage during drying: $\Phi_P = h^{\text{dry}}/h^{\text{wet}}$. The thickness after drying, h^{dry}, has been measured, whereas h^{wet} has been calculated from the film structure assuming an ideal hexagonal structure: $h^{\text{wet}}_{C_{\parallel,2}} = a_0\sqrt{3}$ for $C_{\parallel,2}$. By choosing $\varepsilon_M^{\text{melt}} = 6.5$, the ε_M scale in Fig. 2 was adjusted such that $\tilde{p} = 0.68$ corresponds to $\varepsilon_M = 6.0$. With this simple estimate the measured and calculated phase diagrams can be perfectly matched by the adjustment of a single parameter. In particular, the predicted ε_M value for the onset of the PL phase at $H = 12$ agrees nicely with experiments.

Although based on a rather simple microscopic model, the DDFT simulations correctly predict a phase diagram with intriguing complexity. The large parameter space covered in both simulations and experiments allows us to distinguish the effects of the two constraints being simultaneously present in a thin film situation: the surface field and the film thickness. Our results also reveal the mechanism which shows how both interplay.

Surface fields.—The effect of a single surface is best seen at a large film thickness ($H = 54$). The simulations show that the preferential attraction of one type of block to the surface (the surface field) is sufficient to induce considerable rearrangements of microdomains near the surface, i.e., surface reconstructions. In the middle of the simulation box, cylinders form in all cases. Moving in Fig. 3 from left to right the following surface reconstructions occur for $H = 54$. For $\varepsilon_M \leqslant 2$, A-beads are effectively attracted to the surface and a thin A-wetting layer

(W) forms (which might also be viewed as a half lamella). At $\varepsilon_M \approx 3$, cylinders orient perpendicular to the surface ($C_\perp$). For $\varepsilon_M \approx 4-8$, *A*-beads are weakly repelled from the surface, and cylinders align parallel to the surface ($C_\parallel$). As ε_M is further increased surface reconstructions with noncylindrical microdomains are induced; first a PL, then a lamella (L). In these structures the averaged mean curvature is gradually decreased in order to adopt to the planar symmetry of the surface.

Interference of surface fields.—Our results indicate that surface fields extend into the bulk with a decay length of about one microdomain spacing. Furthermore, they are additive, and for very thin films the effect of both surfaces combines. This explains why, in thin films, a weaker surface field is sufficient to form a PL (or L) than in thick films. It also explains the formation of a PL beneath a wetting layer (W + PL).

Confinement effects modulate the stability regions of phases oriented parallel to the surfaces. An integer multiple of a natural layer thickness is energetically favored. This causes easier deformable phases to occur at intermediate film thicknesses. For very small thicknesses ($H \lesssim$ microdomain size) and weak surface fields, confinement prevents microphase separation and stabilizes a disordered phase (dis).

We note that the orientation behavior of the cylinders is analogous to the phase behavior of lamella-forming diblock copolymers as both are controlled by the interplay between the surface field and confinement effects [24]. Thus, the sequence $C_\parallel \rightarrow C_\perp \rightarrow C_\parallel$ at steps between terraces corresponds to the sequence $L_\parallel \rightarrow L_\perp \rightarrow L_\parallel$ [25]. Also, in cases where the two confining surfaces favor different orientations ($L_\parallel, L_\perp$), the two orientations can coexist and a hybrid (or mixed) structure (HY) forms [26] which is similar to cylinders with necks [11]. We note that in such a HY structure, the bulk microdomain structure is preserved and a grain boundary is stabilized in the thin film by the antisymmetric surface field. Furthermore, a disordered phase has been reported for ultrathin films of lamella-forming diblock copolymers [26] and is in good agreement with our findings. In addition to the alignment effect, hexagonally ordered cylinders can adopt to the planar surface by formation of surface reconstructions (W, PL, L) which also dominate the phase behavior in thin films.

In conclusion, we have identified the deviations from the bulk structure, both in the vicinity of surfaces and in thin films of cylinder-forming block copolymers as surface reconstructions. Together with what is known for lamella-forming systems our results give evidence of a general mechanism governing the phase behavior in thin films of modulated phases: The interplay between the strength of the surface field and the deformability of the bulk structure determines how the system rearranges in the vicinity of the surface. This causes either an orientation of the bulk structure or the formation of surface reconstructions. The stability regions of the different phases are modulated by the film thickness via interference and confinement effects.

This concept along with the presented methods might provide the means to understand and eventually control a wealth of thin film structures in a wide class of ordered fluids, such as linear and star multiblock copolymers as well as surfactant-based fluids.

We thank M. Hund, J. G. E. M. Fraaije, R. A. Segalman, and H. Hänsel for help and discussions, and acknowledge support from the Deutsche Forschungsgemeinschaft (SFB 481) and the NWO-DFG bilateral program.

*To whom correspondence should be adressed.
E-mail: robert.magerle@uni-bayreuth.de

[1] F. S. Bates and G. H. Fredrickson, Annu. Rev. Phys. Chem. **41**, 525 (1990); I. W. Hamley, *The Physics of Block Copolymers* (Oxford University Press, Oxford, 1998).
[2] M. Seul and D. Andelman, Science **267**, 476 (1995).
[3] R. R. Netz, D. Andelman, and M. Schick, Phys. Rev. Lett. **79**, 1058 (1997).
[4] R. A. L. Jones *et al.,* Phys. Rev. Lett. **66**, 1326 (1991).
[5] G. F. Fredrickson, Macromolecules **20**, 2035 (1987).
[6] S. H. Anastasiadis *et al.,* Phys. Rev. Lett. **62**, 1852 (1989).
[7] N. Rehse *et al.,* Phys. Rev. Lett. **87**, 035505 (2001).
[8] For reviews, see, M. W. Matsen, Curr. Opin. Colloid Interface Sci. **3**, 40 (1998); K. Binder, Adv. Polym. Sci. **138**, 1 (1999); M. J. Fasolka and A. M. Mayes, Annu. Rev. Mater. Res. **31**, 323 (2001).
[9] A. Karim *et al.,* J. Chem. Phys. **100**, 1620 (1994).
[10] L. H. Radzilowski, B. L. Carvalho, and E. L. Thomas, J. Polym. Sci. Part B Polym. Phys. **34**, 3081 (1996).
[11] M. Konrad *et al.,* Macromolecules **33**, 5518 (2000).
[12] Ch. Harrison *et al.,* Macromolecules **31**, 2185 (1998); Polymer **30**, 2733 (1998).
[13] Q. Zhang *et al.,* Macromolecules **33**, 9561 (2000).
[14] M. S. Turner, M. Rubinstein, and C. M. Marques, Macromolecules **27**, 4986 (1994).
[15] H. P. Huinink *et al.,* J. Chem. Phys. **112**, 2452 (2000); Macromolecules **34**, 5325 (2001).
[16] G. G. Pereira, Phys. Rev. E **63**, 061809 (2001).
[17] Q. Wang, P. F. Nealy, and J. J. de Pablo, Macromolecules **34**, 3458 (2001).
[18] G. Kim and M. Libera, Macromolecules **31**, 2569 (1998); **31**, 2670 (1998).
[19] T. Hashimoto, M. Shobayama, and H. Kawai, Macromolecules **16**, 1093 (1983).
[20] S. N. Magonov *et al.,* Surf. Sci. **389**, 201 (1997).
[21] A. Knoll, R. Magerle, and G. Krausch, Macromolecules **34**, 4159 (2001).
[22] R. Magerle, Phys. Rev. Lett. **85**, 2749 (2000).
[23] J. G. E. M. Fraaije, J. Chem. Phys. **99**, 9202 (1993); J. G. E. M. Fraaije *et al., ibid.* **106**, 4260 (1997); G. J. A. Sevink *et al., ibid.* **110**, 2250 (1999).
[24] D. G. Walton *et al.,* Macromolecules **27**, 6225 (1994); G. J. Kellogg *et al.,* Phys. Rev. Lett. **76**, 2503 (1996).
[25] B. L. Carvalho and E. L. Thomas, Phys. Rev. Lett. **73**, 3321 (1994).
[26] M. J. Fasolka *et al.,* Macromolecules **33**, 5702 (2000).